# Effect of the Al2O3 Deposition Method on Parylene C: Highlights on a Nanopillar-Shaped Surface

Joanna Njeim, David Alamarguy, Xiaolong Tu, Alan Durnez, Xavier Lafosse, Pascal Chrétien, Ali Madouri, Zhuoxiang Ren, David Brunel

ACS OMEGA

http://pubs.acs.org/journal/acsodf

Article

# Effect of the $Al_2O_3$ Deposition Method on Parylene C: Highlights on a Nanopillar-Shaped Surface

Joanna Njeim, David Alamarguy, Xiaolong Tu, Alan Durnez, Xavier Lafosse, Pascal Chretien, Ali Madouri, Zhuoxiang Ren, and David Brunel*

Cite This: *ACS Omega* 2020, 5, 15828−15834

Read Online

ACCESS | Metrics & More | Article Recommendations | Supporting Information

**ABSTRACT:** Parylene C (PC) has attracted tremendous attention throughout the past few years due to its extraordinary properties such as high mechanical strength and biocompatibility. When used as a flexible substrate and combined with high-$\kappa$ dielectrics such as aluminum oxide ($Al_2O_3$), the $Al_2O_3$/PC stack becomes very compelling for various applications in fields such as biomedical microsystems and microelectronics. For the latter, the atomic layer deposition of oxides is particularly needed as it allows the deposition of high-quality and nanometer-scale oxide thicknesses. In this work, atomic layer deposition (ALD) and electron beam physical vapor deposition (EBPVD) of $Al_2O_3$ on a 15 $\mu$m-thick PC layer are realized and their effects on the $Al_2O_3$/PC resulting stack are investigated via X-ray photoelectron spectroscopy combined with atomic force microscopy. An ALD-based $Al_2O_3$/PC stack is found to result in a nanopillar-shaped surface, while an EBPVD-based $Al_2O_3$/PC stack yields an expected smooth surface. In both cases, the $Al_2O_3$/PC stack can be easily peeled off from the reusable $SiO_2$ substrate, resulting in a flexible $Al_2O_3$/PC film. These fabrication processes are economic, high yielding, and suitable for mass production. Although ALD is particularly appreciated in the semiconducting industry, EBPVD is here found to be better for the realization of the $Al_2O_3$/PC flexible substrate for micro- and nanoelectronics.

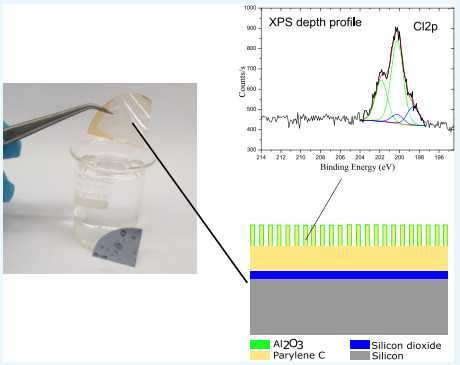


## 1. INTRODUCTION

Poly(*p*-xylylene) $(C_8H_8)_n$ also known as parylene is the name of a family of sustainable and green polymers. Among them, Parylene C (PC) $(C_8H_7Cl)_n$ is the most popular for microelectronic and medical coating applications.[1,2] Deposited via chemical vapor deposition (CVD), this polymer possesses many desirable properties that make it a very versatile material especially in the field of implantable medical devices and electronics.[3,4] For instance, PC is widely used as an encapsulating coating film in a biological environment owing to its high conformability[5,6] and class VI biocompatibility and is United States Food and Drug Administration-approved.[7] As for electronics, PC is broadly employed not only as a dielectric[8,9] but also as a flexible substrate[10,11] in electronics and, in particular, in organic electronics where the deposition process is compatible with organic materials[12] and nanomaterial-based electronics such as carbon nanotubes,[8,13,14] graphene,[15−18] and transition metal dichalcogenides[11,19] where the influence of water molecules is strongly diminished.[20−22]

In order to obtain sub-100 nm electronic devices on top of flexible and biocompatible substrates, electron beam lithography (EBL) becomes mandatory with delicate requirements in terms of flatness of the substrate[23] as well as its resistance to basic solvents and chemicals. PC represents the perfect candidate due to its pinhole and stress-free nature arising from the CVD process as well as its chemical and biological inertness, making it almost completely unaffected by solvents and some basic chemicals.[24] More interestingly, the CVD of PC on top of a rigid host substrate that can be detached *a posteriori* due to the fact that its delamination property in water is a very reliable method of fabricating flexible and EBL-compatible nanodevices.[25,26]

The use of ALD[27,28] of high-$\kappa$ dielectrics is particularly needed in organic and nanoelectronics as it allows the deposition of high-quality and nanometer-scale oxide thicknesses such as $Al_2O_3$ for applications in low-power field-effect transistors[29,30] or in devices with a high-aspect-ratio surface.[31] The ALD technique has thus become the preferred technique in the semiconductor industry.[31]

One of PC's distinguished properties is its easy delamination from the underlying silicon dioxide ($SiO_2$) substrate by simple immersion in deionized (DI) water, as described in Figure 1a. Figure 1b presents the result of the delamination of a 15 $\mu$m-thick PC deposited on a quarter of a 2 in. wafer used in this

**Received:** February 19, 2020
**Accepted:** June 5, 2020
**Published:** June 24, 2020




https://dx.doi.org/10.1021/acsomega.0c00735
*ACS Omega* 2020, 5, 15828−15834

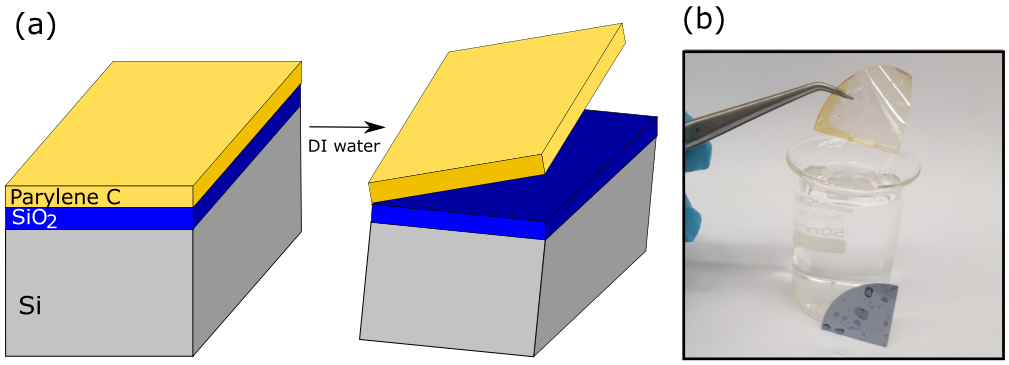


**Figure 1.** (a) Representation of the initial substrate composed of a parylene layer deposited on top of a $SiO_2$/Si substrate before and after delamination. (b) Photograph of the delamination procedure of a 15 $\mu$m-thick PC (yellowish) on a silicon substrate in DI water used in this work. Photograph courtesy of David Brunel. Copyright 2020.

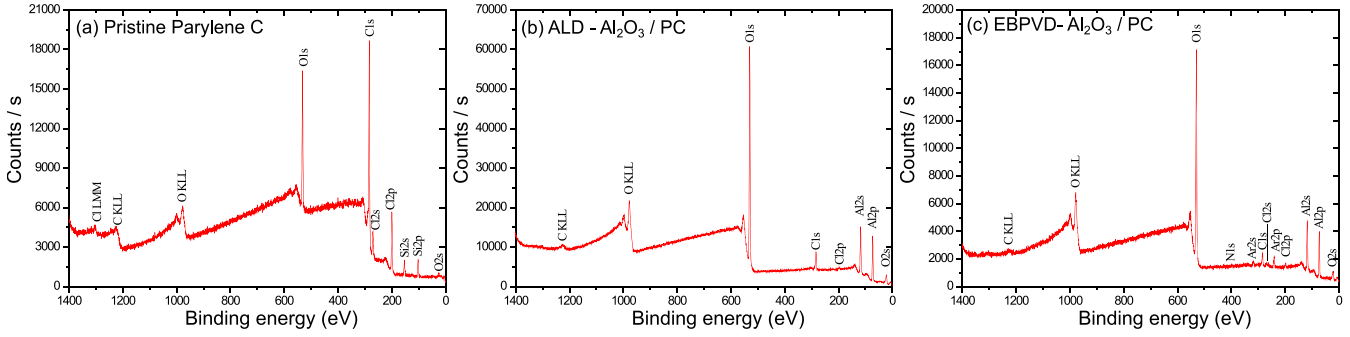


**Figure 2.** XPS spectra of the surface of (a) a pristine PC, (b) ALD-$Al_2O_3$ on PC, and (c) EBPVD-$Al_2O_3$ on PC.

work. The flexible polymer film here is continuous, highly flexible, and transparent. The production and characterization of an $Al_2O_3$-covered PC substrate for flexible micro- and nanoelectronics could lead the path to the realization of large-scale flexible nanoelectronics.

Here, after the CVD of a 15 $\mu$m-thick PC on top of a 285 nm-thick $SiO_2$ substrate (described in the Experimental Section), $Al_2O_3$ is deposited via ALD and EBPVD. The resulting oxide surfaces are analyzed with atomic force microscopy (AFM), and X-ray photoelectron spectroscopy (XPS) is used for a complete analysis of the resulting $Al_2O_3$/PC substrate.

**Table 1. Atomic Concentration of the Elements Detected on the Surface of (a) PC, (b) ALD-$Al_2O_3$/PC, and (c) EBPVD-$Al_2O_3$/PC**

| surface elements | PC | ALD-$Al_2O_3$/PC | EBPVD-$Al_2O_3$/PC |
|---|---|---|---|
| O | 20.3% | 60.2% | 56.8% |
| C | 68.8% | 12.5% | 11.9% |
| Cl | 6.0% | 0.5% | 0.8% |
| Si | 3.9% | 0% | 0% |
| Al | 0% | 26.8% | 25.6% |
| Ar | 0% | 0% | 1.7% |
| N | 0% | 0% | 1.4% |

## 2. RESULTS AND DISCUSSION

**2.1. Surface Characterization.** In this work, a 30 nm-thick $Al_2O_3$ layer is realized with ALD and a 15 nm-thick $Al_2O_3$ with EBPVD on top of PC. The resulted $Al_2O_3$ nanolayers on PC are characterized with XPS (both top surface and depth profiles) combined with AFM. In the literature, investigations of oxide/polymer stacks such as $Al_2O_3$/polypropylene probed with infrared transmission have been realized[32−34] but, to our knowledge, the study of oxide/polymer stack probed by XPS depth profiles is presented for the first time. Figure 2a−c shows the XPS spectra of the surface of (a) a pristine PC, (b) ALD-$Al_2O_3$ on PC, and (c) EBPVD-$Al_2O_3$ on PC. The atomic concentrations of the elements detected on the film surface in each spectrum are collected in Table 1. For a more accurate characterization of the pristine PC away from surface contamination such as adventitious carbon, XPS measurements were carried out on an intentionally but gently scratched area and are presented in Figure 2a. Carbon (C), chlorine (Cl), oxygen (O), and silicon (Si) species are observed on the surface of the pristine PC. The Cl and C atomic concentrations of 6% and 68.8%, respectively, are close to the ones of PC, as one Cl atom is bonded to eight C atoms in a PC monomer. Moreover, the excess of carbon is due to the atmospheric contamination, confirmed by the presence of carbon bonded with hydroxyl groups (C−OH), carbonyl groups (C═O), and carboxyl groups (OH−C═O) in the C 1s spectrum. The detection of silicon with a binding energy at around 103.5 eV for Si 2p, corresponding to $SiO_2$, is certainly due to a previous scratch that has pierced the soft polymer. The remaining 10% oxygen species belong to the standard atmospheric contamination. XPS results of ALD-$Al_2O_3$ on PC are presented in Figure 2b. The presence of Al and O species, with binding energies at 531.2 and 119.3 eV for O 1s and Al 2s, respectively, confirms the conformal deposition of $Al_2O_3$. However, C atoms are also detected on the surface, showing once again the standard carbon−oxygen contamination. XPS measurements were repeated at several regions of the sample, and the


https://dx.doi.org/10.1021/acsomega.0c00735
ACS Omega 2020, 5, 15828−15834

resulting atomic concentrations confirm a homogeneous deposition of $Al_2O_3$.

Figure 2c shows the XPS spectrum of EBPVD-$Al_2O_3$ on PC. Both Al and O are detected on the surface, with binding energies at 531.2 and 119.3 eV for O 1s and Al 2s, respectively, confirming the presence of $Al_2O_3$. In comparison to ALD-deposited $Al_2O_3$, the EBPVD-$Al_2O_3$ contains traces of N on the surface, which are due to the EBPVD process itself, where a nitrogen flux is injected at the end of the deposition process before restoring the atmospheric pressure.

As the flatness of the resulting surface after oxide deposition is crucial in micro- and nanoelectronics, especially when working with a flexible substrate, EBPVD-$Al_2O_3$/PC and ALD-$Al_2O_3$/PC are analyzed via AFM. Figure 3a presents the AFM

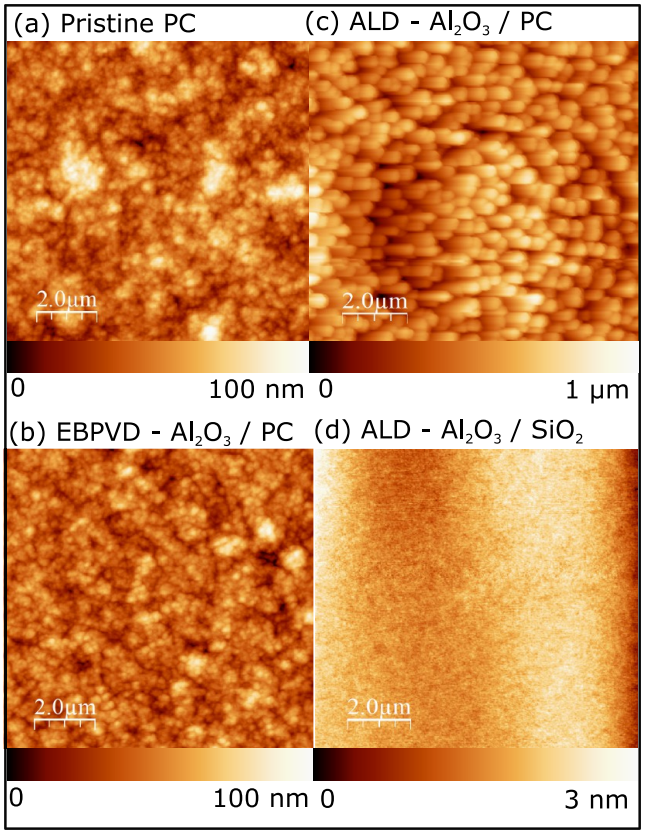


**Figure 3.** AFM images of (a) a 15 $\mu$m-thick pristine PC, (b) EBPVD-$Al_2O_3$ deposited on the pristine PC, (c) ALD-$Al_2O_3$ deposited on the pristine PC, and (d) ALD-$Al_2O_3$ deposited on a 285 nm-thick $SiO_2$ layer.

image of a pristine 15 $\mu$m-thick PC, and the average roughness was measured at ~10 nm with a standard margin error of 15% (see the Experimental Section). Then, EBPVD-$Al_2O_3$/PC is imaged and presented in Figure 3b, where the average roughness is measured at around 10 nm. Hence, the EBPVD process has no effect on the surface roughness of the resulting surface. However, the situation is very different when it comes to ALD-$Al_2O_3$-covered PC, as can be seen in Figure 3c, where a nanopillar-shaped surface is observed with an average and root-mean-square (rms) roughness of 140 and 170 nm, respectively (see the Supporting Information). This observation implies that the ALD of $Al_2O_3$ has strongly impacted the surface of the PC. The ALD technique itself is not responsible for the nanopillar formation, as demonstrated by the deposition of $Al_2O_3$ on a $SiO_2$ substrate and imaged in Figure 3d where a very smooth surface of 0.3 nm rms roughness is measured. The water precursor used to deposit the oxide has perturbed the highly hydrophobic nature of PC and then implied the nanopillar-shaped surface formation.

**2.2. XPS Depth Profiles.** In order to describe the nature of these nanopillars, the XPS depth profile method is used here for an exhaustive characterization of the nanostructured surfaces. First, XPS measurements are calibrated with a known thickness of $Al_2O_3$ deposited with ALD on top of a gold surface (see Figure S1 in the Supporting Information). The quality of this calibration is then confirmed by the EBPVD-$Al_2O_3$ presented in Figure 4a, which depicts the XPS depth profile where the stoichiometry of $Al_2O_3$ is confirmed with expected thickness. Indeed, after the quick disappearance (around 30 s) of the adventitious carbon due to the first sputtering, the oxide is detected for a total sputter time of 10.5 min, corresponding to an oxide thickness of 17 nm, which is in good agreement with a target thickness of 15 nm. The resulting surface can then be simply presented by Figure 4b. Nevertheless, Cl elements, originating from the PC substrate, appear at a sputtering time of 8 min, thus before the disappearance of the $Al_2O_3$, with an inflection point measured at 10.5 min. This implies a reaction between $Al_2O_3$ and the underlying PC, which will be discussed in Figure 5. Concerning the nanopillars, Figure 4c shows the XPS depth profile of the ALD-$Al_2O_3$ on PC. Similar to the EBPVD-$Al_2O_3$, Al and O concentrations verify the redox equation. Nonetheless, the oxide remains detectable for a very long time (~71.8 min), resulting in a thickness of ~144 nm, which is far beyond the theoretical deposited thickness (30 nm) but in the same order of the average roughness measured. It is important to note that ALD-$Al_2O_3$ precursors have been found in the literature to react with the underlying substrate to depths of 100 nm such as with polyamide-6 at 90 °C.[32] Interestingly, Cl species that normally belong to the PC substrate appear after ~15.5 min of sputtering, which corresponds to a thickness of ~31 nm. In addition, the C concentration does not stabilize until the complete disappearance of the oxide (at around 110 min of sputtering). During the oxide deposition, while precursors reacted with PC, a nanopillar-shaped PC surface is formed, and the average height of these nanopillars determined by XPS is consistent with the average roughness measured by AFM. Then, an $Al_2O_3$ layer is covering these nanopillars with a target thickness of 30 nm. The final structure of this nanopillar-shaped surface is presented in Figure 4d.

**2.3. EBPVD-$Al_2O_3$/PC Chemical Structure.** In order to prove the interaction between $Al_2O_3$ and the underlying PC substrate, the Cl 2p, Al 2s, and C 1s peaks were plotted and are shown in Figure 5a–d for EBPVD-$Al_2O_3$ and in Figure 5e–h for ALD-$Al_2O_3$. Concerning the EBPVD-$Al_2O_3$, analyses are focused on sputter times of 10.5 and 19 min marked with a green star and a yellow circle in Figure 4a, whereas for ALD-$Al_2O_3$, analyses are focused on sputter times of 22.5 and 110 min marked with a red square and a blue triangle in Figure 4c, respectively.

The first analysis concerns the yellow circle point that can be considered as the bulk parylene under the EBPVD-$Al_2O_3$. In Figure 5a, the Cl 2p peak is detected after the disappearance of $Al_2O_3$, at 19 min of sputter time. In this case, this peak can be fitted into a single doublet, with two components with binding energies at 200.1 and 201.7 eV, close to values corresponding to chlorine bound to aromatic carbon.[35] Figure 5b presents the


https://dx.doi.org/10.1021/acsomega.0c00735
ACS Omega 2020, 5, 15828−15834

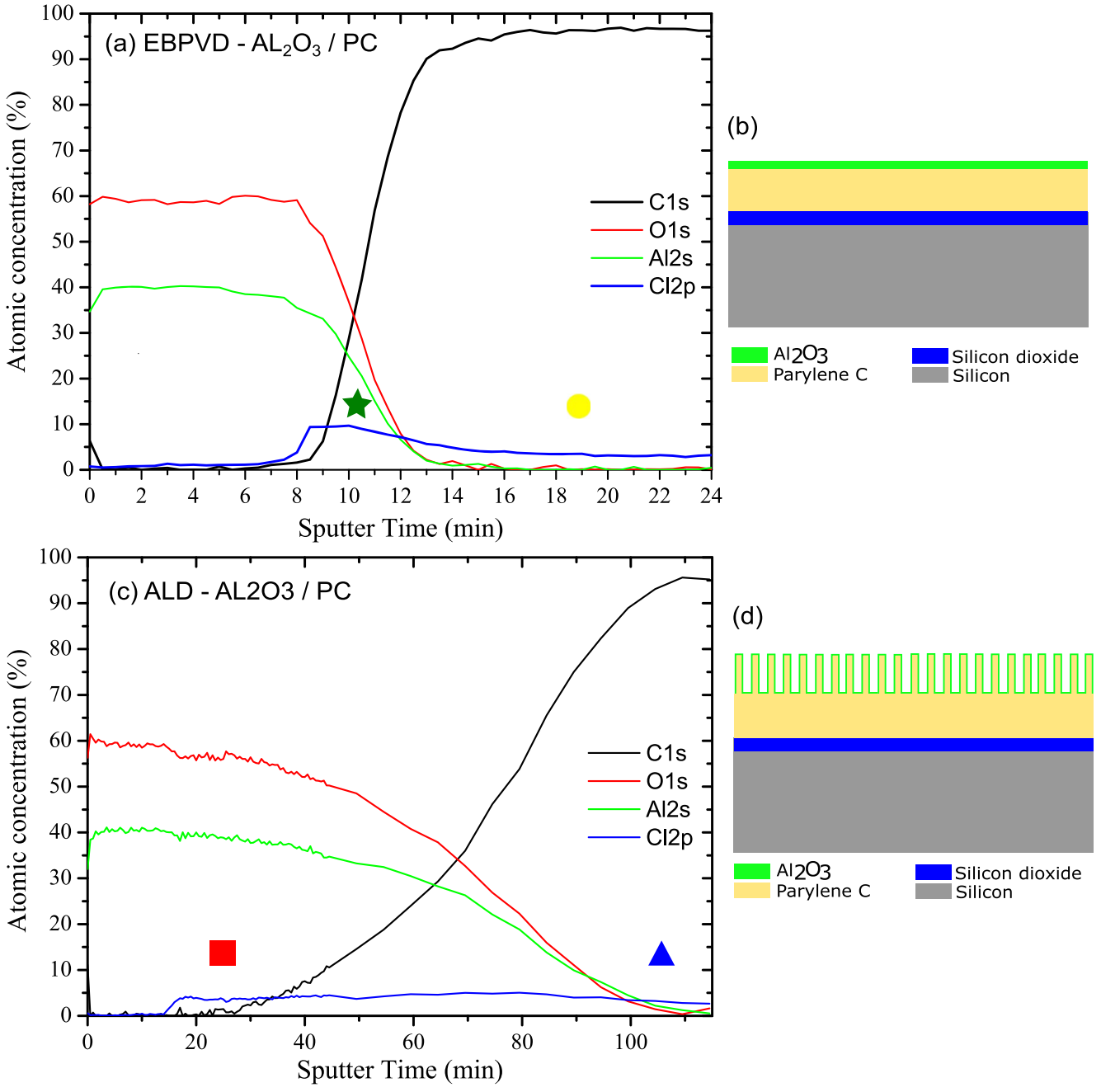


**Figure 4.** (a) XPS depth profile of the EBPVD-$Al_2O_3$ over a 15 $\mu$m-thick PC. (b) Structure of the EBPVD-$Al_2O_3$/PC stack. (c) XPS depth profile of the ALD-$Al_2O_3$ over a 15 $\mu$m-thick PC. (d) Structure of the ALD-$Al_2O_3$/PC stack.

C 1s peak acquired at the same time during the depth profile. This peak can be fitted into two components with binding energies at 284.7 and 286.1 eV, corresponding to aromatic carbon and carbon bound to chlorine, respectively. This first two spectra confirm that the parylene bulk is correctly detected.

Now, we turn to the green star point: the Cl 2p peak is plotted in Figure 5c before the disappearance of the oxide. This Cl 2p peak can be fitted also into a single doublet, with two components observed with binding energies at 198.4 eV (Cl $2p_{3/2}$) and 200.0 eV (Cl $2p_{1/2}$). When these results are compared with the bulk parylene, this shift in Cl 2p binding energies and the change in peak shape due to different full width at half-maxima of the Cl 2p peak before the disappearance of $Al_2O_3$ indicate a reaction between PC and the EBPVD-$Al_2O_3$ layer. The binding energy of this Cl 2p could correspond to $AlCl_3$.[36] To verify this reaction, the Al 2s peak is also plotted in Figure 5d. This peak can be fitted into two components with binding energies at 119.2 and 120.1 eV. The major component, at 119.2 eV, is assigned to $Al_2O_3$.[37] The minor component, at 120.1 eV, could correspond to $AlCl_3$.[38] Thus, when $Al_2O_3$ is deposited with EBPVD on PC, Al atoms react with the PC during the deposition process.

**2.4. ALD-$Al_2O_3$/PC Chemical Structure.** In the following part of this study, we turn to the blue triangle point of ALD-$Al_2O_3$ corresponding to the bulk parylene. Two doublets have been found on the Cl 2p spectrum in Figure 5e (blue triangle), the major doublet with the Cl $2p_{3/2}$ peak at 200.3 eV could


https://dx.doi.org/10.1021/acsomega.0c00735
ACS Omega 2020, 5, 15828−15834

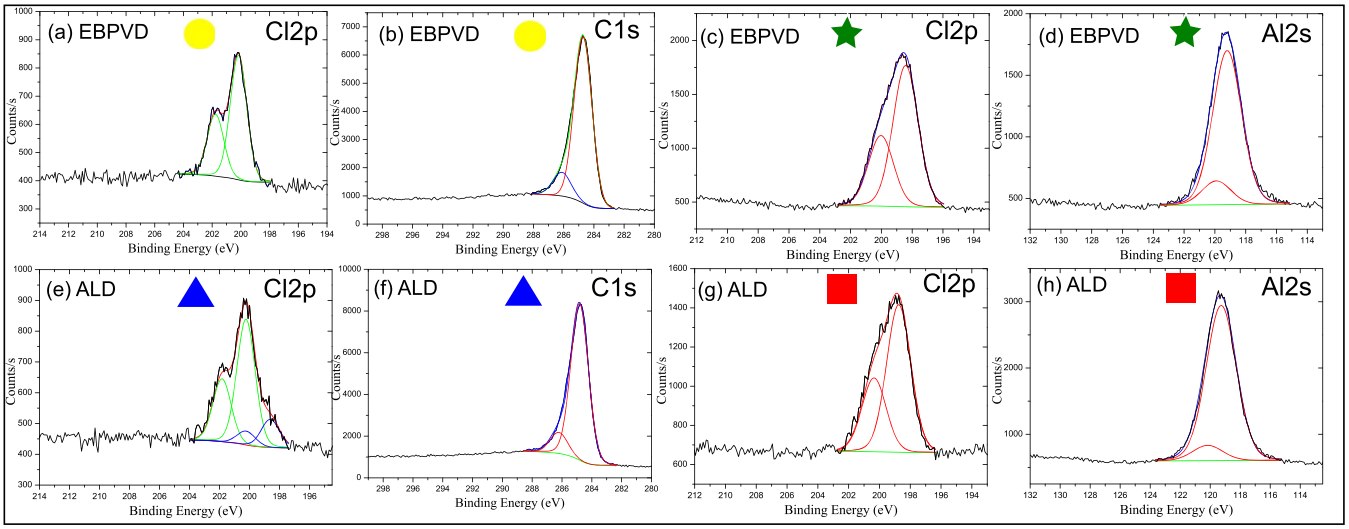


**Figure 5.** (a–d) XPS spectra of EBPVD-$Al_2O_3$/PC at different sputter times marked by colored geometrical forms in Figure 4a: (a) Cl 2p at the yellow circle point, (b) C 1s at the yellow circle point, (c) Cl 2p at the green star point, and (d) Al 2s at the green star point. (e–h) XPS spectra of ALD-$Al_2O_3$/PC at different sputter times marked by colored geometrical forms in Figure 4b: (e) Cl 2p at the blue triangle point, (f) C 1s at the blue triangle point, (g) Cl 2p at the red square point, and (h) Al 2s at the red square point.

correspond to the PC and the minor doublet with the Cl $2p_{3/2}$ peak at 198.7 eV, similar to the one measured on EBPVD-$Al_2O_3$ before the disappearance of the oxide, could also be assigned to $AlCl_3$. This minor doublet is still present certainly because the spectrum has been acquired just after the disappearance of $Al_2O_3$ and thus not completely in the bulk of parylene. However, the C 1s peak was acquired at the same time during the depth profile and is shown in Figure 5f. This peak can be fitted into two components with binding energies at 284.7 and 286.1 eV, corresponding to aromatic carbon and carbon bound to chlorine, respectively, confirming that the major doublet of the Cl $2p_{3/2}$ peak at 200.3 eV corresponds to PC, exactly as seen in Figure 5b.

Finally, the Cl 2p peak in Figure 5g while the oxide is still present is considered and it can be deconvoluted into a single doublet, with two components with binding energies measured at 198.7 eV (Cl $2p_{3/2}$) and 200.3 eV (Cl $2p_{1/2}$). These peaks indicate that ALD-$Al_2O_3$ had also reacted with the underlying PC during the deposition process in the same manner as EBPVD-$Al_2O_3$. Indeed, to prove this assertion, the Al 2s peak is once again plotted in Figure 5h and can be fitted into two components with binding energies of 119.3 and 120.2 eV assigned to $Al_2O_3$ and $AlCl_3$, respectively, exactly as in Figure 5d.

## 3. CONCLUSIONS

EBPVD and ALD of $Al_2O_3$ have been successfully realized on a detachable and flexible PC substrate. Surface characterization was performed via atomic force microscopy, which demonstrated a smooth surface after EBPVD while an unexpected nanopillar-shaped surface was observed after ALD. Extensive investigations have been realized with X-ray photoelectron spectroscopy, and both surface analyses and depth profiles have been studied. Cl 2p, Al 2s, and C 1s peaks have been plotted at key sputter times. The emanating fitting curves indicated for both techniques that PC reacted with the oxide in a similar way. With the ALD technique, the water precursor responsible for the donation of oxygen was found responsible for the strong modification of the substrate roughness since PC is extremely hydrophobic. Combining AFM observations with XPS allowed a complete description of the nanopillar-shaped surface that is indeed high-aspect-ratio nanopillars of PC fully covered with the desired $Al_2O_3$ thickness. These findings are of high value for applications that need flexible and biocompatible substrates such as PC. EBPVD is preferred for realization of micro- and nanodevices based on the $Al_2O_3$/PC substrate, while a nanopillar-shaped surface of $Al_2O_3$-PC is a very interesting substrate for 2D materials such as graphene or $MoS_2$ so as to investigate nanomechanical properties or to increase the carriers' velocity by inhibiting or decreasing the interface interactions with the substrate.

## 4. EXPERIMENTAL SECTION

**4.1. Parylene Deposition.** Silicon substrates (1.5× 1.5 $cm^2$) with a 285 nm-thick thermal $SiO_2$ were coated with 15 $\mu$m-thick PC in a homemade PC coating system. As a reliable deposition process is only obtained for a maximum thickness of 5 $\mu$m, the following process has been repeated three times in order to obtain the needed PC thickness. For every deposition process, the cooling system was started and the pyrolysis chamber was preheated to 690 °C. A total of 8.25 g of PC dimer (1.65 g/$\mu$m according to manufacturer's guide and thickness measurements probed by a stylus profilometer) was transferred to the loading chamber. The deposition process starts when the system pressure is under a critical value of 10 mTorr. At the beginning of the deposition, PC dimers were heated in the loading chamber (~160 °C) and sublimed. The dimer vapor then enters the pyrolysis chamber and is pyrolyzed into monomers. The active monomers polymerize uniformly on any surface they meet in the deposition chamber to form PC. The deposition process stops when all PC dimers are exhausted.

**4.2. Atomic Layer Deposition (ALD) and EBPVD of $Al_2O_3$.** For ALD of $Al_2O_3$, 30 nm-thick $Al_2O_3$ was deposited on PC substrates using a Fiji F200 at 100 °C and under 100 mTorr. This very popular method uses trimethylaluminum (TMA, $Al_2(CH_3)_6$) and water as precursors in the ALD process.[39] Calibration between this deposition method and


https://dx.doi.org/10.1021/acsomega.0c00735
ACS Omega 2020, 5, 15828−15834

XPS measurements was realized using a 26 nm $Al_2O_3$ layer deposited on Au and is described in paragraph 1 of the Supporting information. Here, after a 20 min thermalization required before any deposition, a 1 Å/cycle was realized as follows: Every cycle lasts 60.12 s and is composed of one pulse of TMA of 60 ms followed by 30 s of purging and then 60 ms of $H_2O$ followed by another 30 s of purging. During the purging, an argon flux was pumped into the chamber to eliminate any byproducts or unreacted gases. The deposition time is thus 5 h. The thickness rate was controlled using a quartz microbalance.

For EBPVD of $Al_2O_3$, the RF sputter of $Al_2O_3$ deposition was realized in a Plassys MEB800 IAD (ion-assisted deposition) under a mixture of high-purity argon and oxygen gases with an applied RF power of 300 W. The deposition rate was set at 0.2 nm/s.

**4.3. Surface and Material Characterizations.** Surface topographies were realized using a Bruker Enviroscope atomic force microscopy (AFM). Pixel images (512 × 512) at 0.7 Hz were recorded using tapping mode Budgetsensors AFM probes. Image treatments were realized using WSxM 5.0 Develop 9.1 software from Nanotec Electronica.[40] Average and rms roughness were measured using both WSxM and Nanoscope V softwares.

X-ray photoelectron spectroscopy (XPS) were realized using a PHI 5000 Versaprobe spectrometer (Physical Electronics) operating at a base pressure of $10^{-7}$ Pa. A focused monochromatized Al $K_\alpha$ X-ray source ($h\nu$ = 1486.6 eV) was used at 15 kV. The analyzed area of the sample was 200 $\mu$m in diameter. A dual beam charge neutralization system involving low-energy Ar ions and electrons was used to compensate the charge-up effect. For charge correction, binding energies were calibrated using the C 1s peak from adventitious carbon with a fixed value at 284.8 eV. High-resolution core level spectra were acquired with a 23.5 eV pass energy, an energy step of 0.1 eV, and a 50 ms dwell time. The spectrometer was regularly calibrated with Cu $2p_{3/2}$ and Cu LMM of clean copper at 932.7 and 918.7 eV, respectively. Spectroscopic data were processed by the PHI Multipak software using a peak fitting routine with symmetrical Gaussian−Lorentzian functions. The Shirley background was subtracted from the spectra. The Ar-ion beam conditions for depth profiling were as follows: the ion source was operated at 1 kV, and the raster area was 2 × 2 $mm^2$. Each sputter cycle was set to 30 s, which corresponds to a sputter depth between 0.8 and 1.0 nm in $Al_2O_3$.

## ■ ASSOCIATED CONTENT

### Supporting Information

The Supporting Information is available free of charge at https://pubs.acs.org/doi/10.1021/acsomega.0c00735.

Calibration of ALD-based $Al_2O_3$ deposition, effect of the TMA/water precursors on the nanopillar-shaped surface, and AFM characterization of the nanopillar-shaped surface after ALD-$Al_2O_3$ reaction with parylene C (PDF)

## ■ AUTHOR INFORMATION


### Corresponding Author

**David Brunel** − *Sorbonne Université, CNRS, Laboratoire de Génie Electrique et Electronique de Paris, 75252 Paris, France;* orcid.org/0000-0002-6722-7862; Email: david.brunel@sorbonne-universite.fr

### Authors

**Joanna Njeim** − *Sorbonne Université, CNRS, Laboratoire de Génie Electrique et Electronique de Paris, 75252 Paris, France*

**David Alamarguy** − *Université Paris-Saclay, CentraleSupélec, CNRS, Laboratoire de Génie Electrique et Electronique de Paris, 91192 Gif-sur-Yvette, France*

**Xiaolong Tu** − *Sorbonne Université, PSL Université, Ecole Normale Supérieure, PASTEUR, Département de Chimie, CNRS, 75005 Paris, France*

**Alan Durnez** − *Université Paris-Saclay, CNRS, Centre de Nanosciences et de Nanotechnologies, 91120 Palaiseau, France*

**Xavier Lafosse** − *Université Paris-Saclay, CNRS, Centre de Nanosciences et de Nanotechnologies, 91120 Palaiseau, France*

**Pascal Chretien** − *Université Paris-Saclay, CentraleSupélec, CNRS, Laboratoire de Génie Electrique et Electronique de Paris, 91192 Gif-sur-Yvette, France*

**Ali Madouri** − *Université Paris-Saclay, CNRS, Centre de Nanosciences et de Nanotechnologies, 91120 Palaiseau, France*

**Zhuoxiang Ren** − *Sorbonne Université, CNRS, Laboratoire de Génie Electrique et Electronique de Paris, 75252 Paris, France*

Complete contact information is available at: https://pubs.acs.org/10.1021/acsomega.0c00735


### Author Contributions

The manuscript was written by J.N., D.A., and D.B. and supported by the experimental and theoretical work of all authors. All authors have given approval to the final version of the manuscript.


### Funding

This work was partly supported by the French RENATECH network and by a public grant overseen by the French National Research Agency (ANR) as part of the "Investissements d'Avenir" program (Labex NanoSaclay, reference: ANR-10-LABX-0035).


### Notes

The authors declare no competing financial interest.

## ■ REFERENCES


(1) Henry, D. *Materials and Coatings for Medical Devices: Cardiovascular*; ASM International, Ed.; Materials and processes for medical devices; ASM International: Materials Park, Ohio, 2009.

(2) Pruden, K. G.; Sinclair, K.; Beaudoin, S. Characterization of Parylene-N and Parylene-C Photooxidation. *J. Polym. Sci., Part A: Polym. Chem.* **2003**, *41*, 1486−1496.

(3) Arreaga-Salas, D. E.; Avendaño-Bolívar, A.; Simon, D.; Reit, R.; Garcia-Sandoval, A.; Rennaker, R. L.; Voit, W. Integration of High-Charge-Injection-Capacity Electrodes onto Polymer Softening Neural Interfaces. *ACS Appl. Mater. Interfaces* **2015**, *7*, 26614−26623.

(4) Golda-Cepa, M.; Chorylek, A.; Chytrosz, P.; Brzychczy-Wloch, M.; Jaworska, J.; Kasperczyk, J.; Hakkarainen, M.; Engvall, K.; Kotarba, A. Multifunctional PLGA/Parylene C Coating for Implant Materials: An Integral Approach for Biointerface Optimization. *ACS Appl. Mater. Interfaces* **2016**, *8*, 22093−22105.

(5) Yang, M.; Jeong, S. W.; Chang, S. J.; Kim, K. H.; Jang, M.; Kim, C. H.; Bae, N. H.; Sim, G. S.; Kang, T.; Lee, S. J.; Choi, B. G.; Lee, K. G. Flexible and Disposable Sensing Platforms Based on Newspaper. *ACS Appl. Mater. Interfaces* **2016**, *8*, 34978−34984.

(6) Dahiya, A. S.; Opoku, C.; Poulin-Vittrant, G.; Camara, N.; Daumont, C.; Barbagiovanni, E. G.; Franzò, G.; Mirabella, S.; Alquier, D. Flexible Organic/Inorganic Hybrid Field-Effect Transistors with High Performance and Operational Stability. *ACS Appl. Mater. Interfaces* **2017**, *9*, 573−584.

(7) Uttamchandani, D. Woodhead Publishing series in electronic and optical materials. In *Handbook of MEMS for Wireless and Mobile*

*Applications*; Uttamchandani, D., Ed.; Woodhead Publishing Ltd: Cambridge, 2013.
(8) Artukovic, E.; Kaempgen, M.; Hecht, D. S.; Roth, S.; Grüner, G. Transparent and Flexible Carbon Nanotube Transistors. *Nano Lett.* **2005**, *5*, 757−760.
(9) Sabri, S. S.; Lévesque, P. L.; Aguirre, C. M.; Guillemette, J.; Martel, R.; Szkopek, T. Graphene Field Effect Transistors with Parylene Gate Dielectric. *Appl. Phys. Lett.* **2009**, *95*, 242104.
(10) Fukuda, K.; Takeda, Y.; Yoshimura, Y.; Shiwaku, R.; Tran, L. T.; Sekine, T.; Mizukami, M.; Kumaki, D.; Tokito, S. Fully-Printed High-Performance Organic Thin-Film Transistors and Circuitry on One-Micron-Thick Polymer Films. *Nat. Commun.* **2014**, *5*, 4147.
(11) Chamlagain, B.; Li, Q.; Ghimire, N. J.; Chuang, H.-J.; Perera, M. M.; Tu, H.; Xu, Y.; Pan, M.; Xaio, D.; Yan, J.; Mandrus, D.; Zhou, Z. Mobility Improvement and Temperature Dependence in MoSe2 Field-Effect Transistors on Parylene-C Substrate. *ACS Nano* **2014**, *8*, 5079−5088.
(12) Huang, R.; Tang, Y.; Kuang, Y.; Ding, W.; Zhang, L.; Wang, Y. Resistive Switching in Organic Memory Device Based on Parylene-C With Highly Compatible Process for High-Density and Low-Cost Memory Applications. *IEEE Trans. Electron Devices* **2012**, *59*, 3578−3582.
(13) Aguirre, C. M.; Auvray, S.; Pigeon, S.; Izquierdo, R.; Desjardins, P.; Martel, R. Carbon Nanotube Sheets as Electrodes in Organic Light-Emitting Diodes. *Appl. Phys. Lett.* **2006**, *88*, 183104.
(14) Ganzhorn, M.; Vijayaraghavan, A.; Green, A. A.; Dehm, S.; Voigt, A.; Rapp, M.; Hersam, M. C.; Krupke, R. A Scalable, CMOS-Compatible Assembly of Ambipolar Semiconducting Single-Walled Carbon Nanotube Devices. *Adv. Mater.* **2011**, *23*, 1734−1738.
(15) Kim, M.; Shah, A.; Li, C.; Mustonen, P.; Susoma, J.; Manoocheri, F.; Riikonen, J.; Lipsanen, H. Direct Transfer of Wafer-Scale Graphene Films. *2D Mater.* **2017**, *4*, No. 035004.
(16) Arezki, H.; Boutchich, M.; Alamarguy, D.; Madouri, A.; Alvarez, J.; Cabarrocas, P. R. i.; Kleider, J.-P.; Yao, F.; Hee Lee, Y. Electronic Properties of Embedded Graphene: Doped Amorphous Silicon/CVD Graphene Heterostructures. *J. Phys. Condens. Matter* **2016**, *28*, 404001.
(17) Dalla-Francesca, K.; Noël, S.; Brunel, D.; Houzé, F.; Chrétien, P.; Jaffré, A.; Alamarguy, D. Soft Ultrasonic Exfoliation of Multilayer Graphene for an Application to Electrical Contacts. In *28th International Conference on Electrical Contacts (ICEC 2016)*, Edinburgh, United Kingdom, June 6−9, 2002; Heriot-Watt University: Edinburgh, United Kingdom, 2016; pp 225−230.
(18) Brunel, D.; Berthou, S.; Parret, R.; Vialla, F.; Morfin, P.; Wilmart, Q.; Féve, G.; Berroir, J.-M.; Roussignol, P.; Voisin, C.; Plaçais, B. Onset of Optical-Phonon Cooling in Multilayer Graphene Revealed by RF Noise and Black-Body Radiation Thermometries. *J. Phys. Condens. Matter* **2015**, *27*, 164208.
(19) Gao, J.; Li, B.; Tan, J.; Chow, P.; Lu, T.-M.; Koratkar, N. Aging of Transition Metal Dichalcogenide Monolayers. *ACS Nano* **2016**, *10*, 2628−2635.
(20) Levesque, P. L.; Sabri, S. S.; Aguirre, C. M.; Guillemette, J.; Siaj, M.; Desjardins, P.; Szkopek, T.; Martel, R. Probing Charge Transfer at Surfaces Using Graphene Transistors. *Nano Lett.* **2011**, *11*, 132−137.
(21) Brunel, D.; Levesque, P. L.; Ardiaca, F.; Martel, R.; Derycke, V. Control over the Interface Properties of Carbon Nanotube-Based Optoelectronic Memory Devices. *Appl. Phys. Lett.* **2013**, *102*, No. 013103.
(22) Wang, H.; Wu, Y.; Cong, C.; Shang, J.; Yu, T. Hysteresis of Electronic Transport in Graphene Transistors. *ACS Nano* **2010**, *4*, 7221−7228.
(23) Dey, R. K.; Aydinoglu, F.; Cui, B. Electron Beam Lithography on Irregular Surface Using Grafted PMMA Monolayer as Resist. *Adv. Mater. Interfaces* **2017**, *4*, 1600780.
(24) Meng, E.; Li, P.-Y.; Tai, Y.-C. Plasma Removal of Parylene C. *J. Micromech. Microeng.* **2008**, *18*, No. 045004.
(25) Takeuchi, S.; Ziegler, D.; Yoshida, Y.; Mabuchi, K.; Suzuki, T. Parylene Flexible Neural Probes Integrated with Microfluidic Channels. *Lab Chip* **2005**, *5*, 519.
(26) Tan, C. P.; Craighead, H. G. Surface Engineering and Patterning Using Parylene for Biological Applications. *Materials* **2010**, *3*, 1803−1832.
(27) Tao, J.; Lu, H.-L.; Gu, Y.; Ma, H.-P.; Li, X.; Chen, J.-X.; Liu, W.-J.; Zhang, H.; Feng, J.-J. Investigation of Growth Characteristics, Compositions, and Properties of Atomic Layer Deposited Amorphous Zn-Doped Ga2O3 Films. *Appl. Surf. Sci.* **2019**, *476*, 733−740.
(28) Ma, H.-P.; Yang, J.-H.; Tao, J.-J.; Yuan, K.-P.; Cheng, P.-H.; Huang, W.; Wang, J.-C.; Guo, Q.-X.; Lu, H.-L.; Zhang, D. W. Low-Temperature Epitaxial Growth of High-Quality GaON Films on ZnO Nanowires for Superior Photoelectrochemical Water Splitting. *Nano Energy* **2019**, *66*, 104089.
(29) Chang, H.-Y.; Yang, S.; Lee, J.; Tao, L.; Hwang, W.-S.; Jena, D.; Lu, N.; Akinwande, D. High-Performance, Highly Bendable $MoS_2$ Transistors with High-K Dielectrics for Flexible Low-Power Systems. *ACS Nano* **2013**, *7*, 5446−5452.
(30) Bergeron, H.; Sangwan, V. K.; McMorrow, J. J.; Campbell, G. P.; Balla, I.; Liu, X.; Bedzyk, M. J.; Marks, T. J.; Hersam, M. C. Chemical Vapor Deposition of Monolayer $MoS_2$ Directly on Ultrathin $Al_2O_3$ for Low-Power Electronics. *Appl. Phys. Lett.* **2017**, *110*, No. 053101.
(31) Walton, S. G.; Greene, J. E. Plasmas in Deposition Processes. In *Handbook of Deposition Technologies for Films and Coatings*; Elsevier, 2010; pp 32−92, DOI: 10.1016/B978-0-8155-2031-3.00002-8.
(32) Spagnola, J. C.; Gong, B.; Arvidson, S. A.; Jur, J. S.; Khan, S. A.; Parsons, G. N. Surface and Sub-Surface Reactions during Low Temperature Aluminium Oxide Atomic Layer Deposition on Fiber-Forming Polymers. *J. Mater. Chem.* **2010**, *20*, 4213.
(33) Gong, B.; Peng, Q.; Jur, J. S.; Devine, C. K.; Lee, K.; Parsons, G. N. Sequential Vapor Infiltration of Metal Oxides into Sacrificial Polyester Fibers: Shape Replication and Controlled Porosity of Microporous/Mesoporous Oxide Monoliths. *Chem. Mater.* **2011**, *23*, 3476−3485.
(34) Jur, J. S.; Spagnola, J. C.; Lee, K.; Gong, B.; Peng, Q.; Parsons, G. N. Temperature-Dependent Subsurface Growth during Atomic Layer Deposition on Polypropylene and Cellulose Fibers. *Langmuir* **2010**, *26*, 8239−8244.
(35) Beamson, G.; Briggs, D. High Resolution XPS of Organic Polymers: The Scienta ESCA300 Database (Beamson, G.; Briggs, D.). *J. Chem. Educ.* **1993**, *70*, A25.
(36) Hosono, E.; Fujihara, S.; Kimura, T. Fabrication and Electrical Properties of Micro/Nanoporous ZnO : Al Films. *J. Mater. Chem.* **2004**, *14*, 881.
(37) Moulder, J. F.; Stickle, W. F.; Sobol, P. E.; Bomben, K. D. *Handbook of X-Ray Photoelectron Spectroscopy. Physical Electronics*, Perkin-Elmer Corporation-Physical Electronics Division; Jill Chastain: Eden Prairie, Minnesota, 1995.
(38) Wang, B.; Zhang, L.; Su, Y.; Mou, X.; Xiao, Y.; Liu, J. Investigation on the Corrosion Behavior of Aluminum Alloys 3A21 and 7A09 in Chloride Aqueous Solution. *Mater. Des.* **2013**, *50*, 15−21.
(39) Salami, H.; Poissant, A.; Adomaitis, R. A. Anomalously High Alumina Atomic Layer Deposition Growth per Cycle during Trimethylaluminum Under-Dosing Conditions. *J. Vac. Sci. Technol. Vac. Surf. Films* **2017**, *35*, 01B101.
(40) Horcas, I.; Fernández, R.; Gómez-Rodríguez, J. M.; Colchero, J.; Gómez-Herrero, J.; Baro, A. M. WSXM: A Software for Scanning Probe Microscopy and a Tool for Nanotechnology. *Rev. Sci. Instrum.* **2007**, *78*, No. 013705.


https://dx.doi.org/10.1021/acsomega.0c00735
*ACS Omega* 2020, 5, 15828−15834